RESEARCH PAPER

Molecular Engineering of a Ru_2Gd_3 Hetero-Pentanuclear Complex for Dual MRI Relaxivity and Photocatalytic Rhodamine B Degradation

[1]M. Umadevi, [2*]T. Lurthu Pushparaj, [3]E. Francy Irudaya Rani

[1]Research Scholar, PG & Research Department of Chemistry, T.D.M.N.S. College, Affiliated to Manonmanium Sundaranar University, Tamilnadu-627113, India.

[*2]Assistant Professor and the Head, PG and Research Department of Chemistry, T.D.M.N.S. College, Affiliated to Manonmanium Sundaranar University, Tamil Nadu-627113, India

[3]Assistant Professor, Department of Electronics and Communication Engineering, Francis Xavier Engineering College, Affiliated to Anna University, Tamil Nadu-627003, India

**Email ID: chemlurthu2006@gmail.com*

****Corresponding Author: T. Lurthu Pushparaj****

Abstract

A heterometallic Ru(II)–Gd(III) supramolecular complex incorporating photoactive ruthenium(II) polypyridyl units and gadolinium(III)–DO3A coordination centres was investigated for its magnetic relaxation properties and visible-light-driven photocatalytic activity. The longitudinal and transverse proton relaxation behaviours were evaluated at different complex concentrations to explore its potential as a multifunctional MRI contrast agent. The complex exhibited a longitudinal relaxivity (r_1p) of 26.43 mM^{-1} s^{-1}, corresponding to 8.81 mM^{-1} s^{-1} per Gd(III) centre, demonstrating improved per-gadolinium relaxivity compared with several conventional mononuclear Gd(III) complexes. The reported transverse relaxivity (r_2p) was 37.61 mM^{-1} s^{-1}, with an r_2p/r_1p ratio of 1.42, suggesting potential for T_1-weighted MRI applications. Furthermore, the longitudinal relaxivity increased to 54.61 mM^{-1} s^{-1} in phosphate-buffered saline containing 4.5% human serum albumin (HSA), approximately 2.06 times higher than in the absence of HSA. The albumin association constant was determined to be 6917 ± 658 M^{-1}, indicating favourable protein interaction. Additionally, the complex demonstrated visible-light-induced photocatalytic activity towards Rhodamine B (RhB) degradation. A dye–catalyst binding constant of 3.45×10^4 M^{-1} and a pseudo-first-order rate constant of 0.052 min^{-1} indicated favourable substrate interaction and degradation kinetics. The photocatalytic behaviour is attributed to photoinduced metal-to-ligand charge transfer and subsequent reactive oxygen species generation. The findings highlight the potential of the Ru(II)–Gd(III) supramolecular system for further investigation in MRI contrast enhancement and environmental photocatalysis.

Keywords: Ru(II)–Gd(III) heterotetranuclear complex, MRI relaxivity, visible-light photocatalysis, Rhodamine B Dye, LCT and MLCT, wastewater treatment.

How to cite this article: 1M. Umadevi 2*T. Lurthu Pushparaj 3E. Francy Irudaya Rani. Molecular Engineering of a Ru2Gd3 Hetero-Pentanuclear Complex for Dual MRI Relaxivity and Photocatalytic Rhodamine B Degradation. Int J Drug Deliv Technol. 2026;16(90s):2056-2067. DOI: 10.25258/ijddt.16.90s.205.

1. Introduction

Magnetic resonance imaging (MRI) is a widely employed non-invasive diagnostic technique for examining internal organs, soft tissues, blood vessels, and pathological conditions. MRI contrast agents are administered to improve image quality by modifying the relaxation behaviour of surrounding water protons. Based on their effects on image intensity, these agents are broadly classified as positive (T_1-weighted) and negative (T_2-weighted) contrast agents. Gadolinium-based chelates, iron oxide nanoparticles, and manganese-containing compounds are among the important classes of MRI contrast materials. Gadolinium(III) complexes are particularly important because of their strong paramagnetic properties, which enhance longitudinal relaxation and produce increased signal intensity in T_1-weighted images. Depending on their molecular architecture, gadolinium chelates are classified as linear and macrocyclic complexes, while their biological distribution includes extracellular, blood-pool, and organ-specific agents [1–3]. The coordination environment and stability of these complexes are important considerations in the development of safer and more efficient contrast agents. Recently, considerable attention has been directed towards multifunctional metal complexes capable of combining magnetic resonance and optical imaging. Ruthenium(II) polypyridyl complexes exhibit characteristic luminescence, relatively long excited-state lifetimes, and favourable photophysical properties, whereas gadolinium(III) complexes provide paramagnetic characteristics suitable for MRI applications. Combining these complementary properties offers opportunities for developing dual-modal imaging materials. A researcher reported a heterobimetallic Ru(II)–Gd(III) complex comprising a luminescent $[Ru(bpy)_2(phen)]^{2+}$ unit and a DOTA-coordinated Gd(III) centre. The complex exhibited water solubility, low cytotoxicity, strong luminescence, and a longitudinal relaxivity of 4.71 mM^{-1} s^{-1}, demonstrating its potential for T_1-weighted MRI and

luminescence imaging [4-6]. Such developments highlight the significance of transition-metal and lanthanide coordination chemistry in multifunctional biomedical applications.

Beyond biomedical imaging, metal complexes and nanostructured materials have gained considerable importance in environmental remediation, particularly for photocatalytic degradation of organic pollutants. Industrial activities associated with textile, pharmaceutical, leather, paper, printing and dye-manufacturing sectors generate substantial quantities of coloured wastewater. Synthetic dyes, particularly azo and anthraquinone derivatives, possess complex chemical structures and may resist conventional biological treatment. Their discharge into aquatic environments can interfere with light penetration and photosynthetic activity, while certain dyes and their transformation products may exhibit toxic, mutagenic, or carcinogenic characteristics [7,8]. Consequently, developing efficient methods for removing persistent dye pollutants from wastewater is an important environmental objective. Photocatalysis is an advanced oxidation process that utilizes light energy to initiate chemical reactions for pollutant degradation. In heterogeneous semiconductor photocatalysis, irradiation with photons of sufficient energy promotes electrons from the valence band to the conduction band, generating electron–hole pairs. These charge carriers participate in oxidation and reduction reactions at the catalyst surface, producing reactive oxygen species, particularly hydroxyl radicals (•OH) and superoxide radicals ($\bullet O_2^-$). These reactive intermediates attack organic dye molecules, resulting in their progressive decomposition into smaller compounds and, under favourable conditions, eventual mineralization into carbon dioxide, water and inorganic species [8-10]. The effectiveness of photocatalysis depends on factors such as catalyst composition, band-gap energy, surface area, pH, initial dye concentration, catalyst dosage, irradiation intensity and exposure time. Electron–hole recombination is another important limitation because it reduces the availability of charge carriers for surface reactions.

Based on their composition and structural arrangement, semiconductor photocatalysts have also been classified into three generations. First-generation materials generally comprise single-component semiconductors, such as titanium dioxide (TiO_2) and zinc oxide (ZnO). Second-generation photocatalysts include modified and multicomponent semiconductor systems designed to improve visible-light absorption and charge separation. Third-generation materials involve photocatalysts dispersed or immobilized on suitable supporting substrates, facilitating catalyst recovery and reuse. These classifications provide a useful framework for understanding the development of photocatalytic materials and their application in dye-contaminated wastewater treatment [11-13]. In addition to conventional semiconductor materials, transition-metal complexes, lanthanide-containing compounds and metal oxide nanostructures have been investigated for their photochemical and catalytic properties. Gadolinium-based materials have attracted interest in the degradation of organic dyes, including Rhodamine B, while ruthenium complexes are of interest because of their characteristic electronic transitions and light-responsive properties. The photocatalytic behaviour of these materials depends on their coordination environment, electronic structure, light absorption, and interaction with pollutant molecules [14-16]. Different metal-based systems have been investigated for degrading dyes such as methyl orange (MO), methyl green (MG), Rhodamine B (RhB), acid orange 7 (AO7) and acid yellow 23 (AY23) under suitable irradiation conditions. The generation of hydroxyl and superoxide radicals is particularly important in these degradation processes. Furthermore, combining metal oxides with hydrogen peroxide under UV irradiation can enhance reactive radical production and promote pollutant oxidation [17-21]. The complementary properties of transition-metal and lanthanide coordination compounds, ruthenium- and gadolinium-based materials, provide interesting opportunities in functional inorganic chemistry. Although Ru(II)–Gd(III) heterobimetallic complexes (Fig.1) have demonstrated potential in dual-modal biomedical imaging, the photocatalytic performance of appropriate Ru- and Gd-containing materials requires independent investigation. Exploring their structural, optical, and catalytic properties may contribute to the development of multifunctional metal-based materials and efficient strategies for the degradation of organic pollutants.

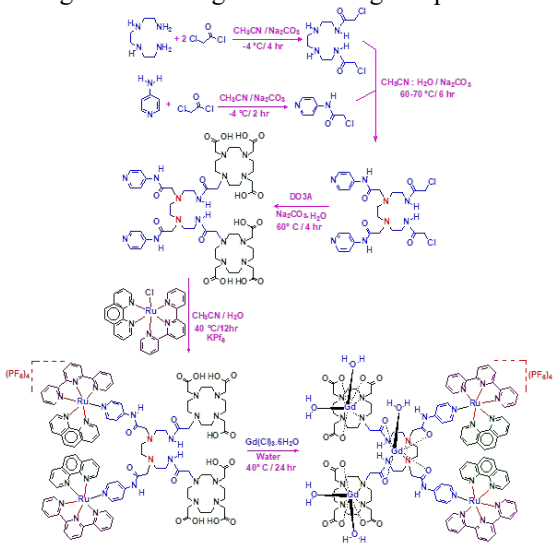

Figure-1. The image shows the step-wise synthetic scheme of the work

2. Literature review and research gap

The development of multifunctional heterometallic coordination complexes has attracted considerable interest because of their ability to integrate different physicochemical properties within a single molecular architecture. Among transition-metal complexes, ruthenium(II) polypyridyl compounds are particularly attractive owing to their intense metal-to-ligand charge-transfer (MLCT) absorption, visible-light responsiveness, and favourable photophysical properties. Gadolinium(III), with its seven unpaired 4f electrons, is extensively employed in magnetic resonance imaging (MRI) contrast-agent development because of its ability to enhance the relaxation rates of surrounding water protons. Consequently, combining Ru(II) photosensitizing units with Gd(III) chelating centers offers an interesting strategy for developing multifunctional molecular systems. Several investigations have demonstrated the potential of Ru(II)–Gd(III) heterometallic complexes for combined magnetic resonance and optical imaging. Caravan et al. [20] discussed how molecular structure, water coordination, and rotational dynamics determine the relaxivity of Gd(III)-based MRI contrast agents. Shi et al. [4] developed a heterobimetallic Ru(II)–Gd(III) magnetoluminescent complex incorporating $[Ru(bpy)_2(phen)]^{2+}$ and a DOTA–Gd(III) unit. The complex exhibited a longitudinal relaxivity (r_1) of 4.71 mM^{-1} s^{-1} and demonstrated potential for T_1-weighted MRI and luminescence imaging. Similarly, Nithyakumar and Alexander [22,23] reported a Ru(II)–$Gd(III)_2$ heterotrimetallic complex with a per-Gd longitudinal relaxivity of 5.80 mM^{-1} s^{-1} in aqueous solution, which increased to 14.30 mM^{-1} s^{-1} in the presence of human serum albumin (HSA). Subsequent studies reported tri- and tetranuclear Ru(II)–Gd(III) complexes with promising relaxometric and optical properties, demonstrating how molecular architecture influences MRI performance [2,22]. These studies established the feasibility of integrating ruthenium-based optical properties with gadolinium-mediated proton relaxation. In parallel, photocatalytic degradation of organic pollutants has emerged as an important approach for wastewater treatment. Rhodamine B (RhB) is frequently employed as a model organic dye because of its intense visible absorption and persistence in aqueous environments. Ruthenium polypyridyl complexes are particularly interesting for photocatalytic applications because their MLCT excited states can facilitate photoinduced electron-transfer processes and potentially promote reactive oxygen species formation under suitable conditions. Despite these developments, the integration of MRI relaxivity evaluation with photocatalytic dye degradation in the same molecular system remains an interesting research opportunity. In particular, the influence of RhB association and solution pH on the magnetic relaxation behaviour of a Ru–Gd heterometallic complex, alongside its photocatalytic performance, deserves further investigation.

3. Experimental Section

3.1 Chemicals Needed: The chemicals required for the present study include 2-aminopyridine, triethylenetetramine, 2-chloroacetyl chloride, cyclen, gadolinium(III) chloride hexahydrate [$GdCl_3 \cdot 6H_2O$], ruthenium(III) chloride hydrate [$RuCl_3 \cdot xH_2O$], sodium carbonate, sodium bicarbonate, sodium hydroxide, potassium hydroxide, triethylamine. The solvents used include acetonitrile (AR), ethanol (AR), methanol (AR), chloroform (AR), acetone (AR), dimethylformamide (DMF), dimethyl sulfoxide (DMSO) and triple-distilled water. Reactive Rhodamine B Dye (RBD) will be used as the dye for photocatalytic degradation studies. Ammonium persulfate, potassium persulfate, hydrochloric acid, sulfuric acid, isopropyl alcohol, tert-butanol, and benzoquinone. For physicochemical analysis of wastewater, potassium dichromate, silver sulfate, mercuric sulfate, manganous sulfate, sodium thiosulfate, starch indicator, phosphate buffer, magnesium sulfate, calcium chloride, ferric chloride, silver nitrate, potassium chromate, barium chloride, ammonium molybdate, ascorbic acid, and potassium hydrogen phthalate were also used. Potassium bromide (KBr) and deuterated solvents such as DMSO-d_6, D_2O, and $CDCl_3$ were used for spectroscopic characterization, wherever applicable.

3.2. Methods

3.2.1. Physical Measurements.

Elemental analyses (C, H, N, and O) were performed using a Perkin-Elmer 2400 Series II CHNS/O elemental analyzer coupled with a Perkin-Elmer AD 8 automatic balance. High-purity argon gas (99.99%) was employed as the carrier gas. FT-IR spectra were collected using a Perkin-Elmer FT-IR spectrometer over the wavenumber range of 4000–400 cm^{-1}. Solid-state samples were analyzed as potassium bromide (KBr) pellets. The 1H and 13C NMR spectra were acquired using a Bruker AVANCE III 500 MHz multinuclear NMR spectrometer. A 5 mm broadband gradient BBO probe was employed for 1H NMR measurements, whereas a 5 mm inverse QXI probe was used to record the 13C NMR spectra. Electrospray ionization mass spectra (ESI-MS) were obtained using a Micromass Quattro II triple-quadrupole mass spectrometer. Samples were dissolved in appropriate solvents and introduced into the ionization source using a syringe pump at a flow rate of 5 µL min^{-1}. The ESI capillary voltage and cone voltage were maintained at 3.5 kV and 40 V, respectively. The reported mass spectra represent the average of seven to nine scans. Electronic absorption spectra were recorded using a Perkin-Elmer UV–Visible spectrophotometer operated with M. Wave Professional 2.0 software. Measurements were

carried out over the wavelength range of 200–900 nm at 25 °C using matched quartz cuvettes fitted with Teflon stoppers and having a 1 cm optical path length. The sample concentration and solvent composition were maintained consistently during the spectral measurements.

3.3. Relaxivity Measurements

3.3.1. Longitudinal and Transverse Relaxivity Measurements: The longitudinal (T_1) and transverse (T_2) relaxation times of the synthesized Ru(II)–Gd(III) metal complex will be measured using a 20 MHz NMR relaxometer at a controlled temperature of 37 ± 0.1 °C. A series of aqueous solutions containing different concentrations of the synthesized metal complexes will be prepared using triple-distilled water. The pH of the solutions will be maintained at approximately 7. The longitudinal relaxation times will be determined using an appropriate inversion-recovery or saturation-recovery pulse sequence, whereas the transverse relaxation times will be measured using the Carr–Purcell–Meiboom–Gill (CPMG) pulse sequence. All measurements will be performed under identical experimental conditions.

The longitudinal and transverse relaxation rates (R_1) and (R_2) will be calculated from the reciprocal of the corresponding relaxation times using the following equations: $R_1=1/T_1$ and $R_2=1/T_2$. The longitudinal (r_1) and transverse (r_2) relaxivities will be determined from the slopes of the linear plots of R_1 and R_2, respectively, against the molar concentration of the metal complexes. $R_1=R_1^0 + r_1[C]$ and $R_2=R_2^0 + r_2[C]$, where (R_1^0) and (R_2^0) represent the relaxation rates of the solvent in the absence of the paramagnetic complex, and [C] represents the molar concentration of the complex. The relaxivity values will be expressed in $mM^{-1}\ s^{-1}$. For polynuclear gadolinium complexes, both molecular relaxivity and relaxivity per Gd(III) ion will be calculated.

3.3.2. Relaxivity Measurements in the Presence of Human Serum Albumin (HSA): The interaction of the synthesized Gd(III) complexes with human serum albumin (HSA) will be investigated by measuring their longitudinal and transverse relaxation properties in the presence of the protein. Aqueous solutions of HSA will be prepared at suitable concentrations using an appropriate buffer medium. Different concentrations of the synthesized metal complexes will be added to the HSA solutions, and the mixtures will be incubated at 37 ± 0.1 °C to facilitate protein–complex interaction. The T1 and T2 relaxation times will be measured using the 20 MHz NMR relaxometer employing appropriate inversion-recovery and CPMG pulse sequences, respectively. The corresponding relaxation rates and relaxivities will be calculated and compared with those obtained in aqueous solution without HSA. Changes in relaxivity will be evaluated to understand the influence of protein binding, molecular tumbling and the accessibility of coordinated water molecules on the relaxation behaviour of the synthesized complexes. The results will provide information about the potential of the complexes as MRI contrast-enhancing agents under protein-containing biological conditions.

3.3.3. Relaxivity Measurements in PBS buffer: The influence of solution pH on the longitudinal and transverse relaxivities of the synthesized metal complexes will be investigated using aqueous solutions maintained in PBS. The concentration will be adjusted to six different concentrations using PBS buffer solutions. The metal complexes will be dissolved at predetermined concentrations, and their T1 relaxation times will be measured using the 20 MHz NMR relaxometer at 37 ± 0.1 °C. The corresponding R1 values will be calculated, and the relaxivities will be evaluated to determine the influence of pH on the relaxation properties of the complexes. Variations in relaxivity may provide information about changes in the coordination environment, water accessibility, and chemical stability of the metal complexes under different solution conditions. Particular attention will be given to the stability of Gd(III) complexes under PBS conditions.

3.3.4. Photocatalytic analysis: Rhodamine B (RhB), a synthetic xanthene-based cationic dye, will be used as the model organic pollutant for evaluating the photocatalytic activity of the synthesized metal complexes. Aqueous RhB solutions of known concentrations will be prepared using triple-distilled water. The photocatalytic degradation of RhB will be monitored using a UV–Visible spectrophotometer by measuring its characteristic absorption maximum at approximately 554 nm. The initial absorbance (A_0) and the absorbance after irradiation for a specified time (A_t) will be recorded to determine the percentage of dye degradation using the following equation:

$$\text{Degradation (\%)} = [(A_0 - A_t) / A_0] \times 100$$

The photocatalytic experiments will be conducted using the synthesized Ru(II), Gd(III), and Ru(II)–Gd(III) metal complexes under suitable UV or visible-light irradiation. The influence of catalyst dosage, initial dye concentration, solution pH, and irradiation time will be investigated. Before irradiation, the catalyst suspension will be stirred in the dark to establish adsorption–desorption equilibrium. At predetermined intervals, aliquots will be withdrawn and centrifuged to remove suspended catalyst particles before measuring the residual dye concentration. Appropriate control experiments will also be performed to distinguish photolysis, adsorption, and photocatalytic degradation.

3.4 Preparation of 4.5% (w/v) HSA and Ru(II)–Gd(III) complex /HSA samples.

HSA was dissolved in a 10 mM sodium phosphate and 150 mM sodium chloride (pH = 7.4)

solution. Two HSA solutions (4.5% w/v) were made: one containing the Ru(II)–Gd(III) complex at a concentration of 1.0 mM and the other without the complex.

3.5. Synthesis and Characterization of ligand and complex.

3.5.1. Synthesis of 2- Chloro-N-(pyridine-4-yl) acetamide (CPA): A stirred solution of 4-aminobenzoic acid (1.37 g, 10.0 mmol) and sodium carbonate (1.27 g, 12.0 mmol) was prepared in a mixture of acetonitrile and water (1:1, v/v, 30 mL) and cooled to −4 °C using an ice–salt bath. A solution of Chloroacetyl chloride (0.88 mL, 11.0 mmol) in dry acetonitrile (5 mL) was added dropwise over 20 min, while maintaining the internal reaction temperature below 0 °C. The reaction mixture was then stirred at −4 °C for 2 h. The progress of the reaction was monitored by thin-layer chromatography (TLC) using dichloromethane/methanol (9:1, v/v) as the eluent. Upon completion, the reaction mixture was acidified to approximately pH 2 using cold 1 M aqueous hydrochloric acid. The resulting precipitate was collected by vacuum filtration, washed with ice-cold water (3 × 15 mL), followed by cold diethyl ether (10 mL), and dried under vacuum at 40 °C to afford CPA as a white solid (1.81 g, 85% yield). The melting point was determined to be 239 °C. ^{1}H NMR (400 MHz, DMSO-d_6) δ 12.75 (br s, 1H, COOH), 10.60 (s, 1H, NH), 7.90 (d, J = 8.8 Hz, 2H, ArH), 7.70 (d, J = 8.8 Hz, 2H, ArH), 4.30 (s, 2H, CH2Cl); ^{13}C NMR (100 MHz, DMSO-d6) δ 167.3, 165.2, 142.8, 130.8, 126.2, 119.1, 43.8; IR (KBr, cm−1): ν 3310 (N–H), 2820–3080 (O–H), 1682 (C=O for COOH), 1665 (C=O for amide), 1532 (N–H); HRMS (ESI-TOF): m/z: [M + H]+ calcd for $C_9H_9ClNO_3$, 214.0265.

3.5.2. Synthesis of Triethylene tetramine (Bis-amide) (TETBA): To a stirred solution of N, N′-((ethane-1,2-diylbis(azanediyl))bis(ethane-2,1-diyl))bis(2-aminoacetamide) (2.60 g, 10.0 mmol) and sodium carbonate (2.54 g, 24.0 mmol) in a mixture of acetonitrile and water (1:1, v/v, 40 mL), cooled to −4 °C using an ice–salt bath, a solution of Chloroacetyl chloride (1.75 mL, 22.0 mmol, 2.2 equiv.) in dry acetonitrile (10 mL) was added dropwise over 30 min. Throughout the addition, the internal reaction temperature was maintained below 0 °C. The reaction mixture was subsequently stirred at −4 °C for 4 h. Upon completion of the reaction, the volatile organic solvent was removed under reduced pressure. The resulting crude product was washed with cold diethyl ether (15 mL) and dried under vacuum at 40 °C to afford TETBA as an off-white solid (3.30 g, 80% yield). The melting point was determined to be 172–174 °C. ^{1}H NMR (400 MHz, DMSO-d_6) δ 8.52 (t, J = 5.6 Hz, 2H, amide NH), 8.12 (t, J = 5.6 Hz, 2H, amide NH), 4.12 (s, 4H, $ClCH_2$), 3.68 (d, J = 5.6 Hz, 4H, $COCH_2NH$), 3.14 (q, J = 6.0 Hz, 4H, CH_2NH), 2.58–2.50 (m, 8H, central TETA CH_2); ^{13}C NMR (100 MHz, DMSO-d6) δ 169.1, 166.8, 48.5, 48.0, 42.6, 42.1, 38.8; IR (KBr, cm^{-1}) ν 3295 (N–H stretch), 1658 (C=O, amide I), 1545 (N–H bend, amide II), 785 (C–Cl); HRMS (ESI-TOF) m/z: $[M + H]^+$ calculated for $C_{14}H_{29}Cl_2N_6O_4$, 413.1622; found, 413.1628.

3.5.3. Synthesis of (4-pyridinyl) acetamido) appended Triethylene tetramine (Bis-amide) (TETBA-PA): TETBA compound (4.13 g, 10.0 mmol) and sodium carbonate (Na_2CO_3) (2.54 g, 24.0 mmol) were suspended in a mixture of acetonitrile and water (1:1, v/v, 50 mL) and heated at 60-70 °C in a heating mantle. A solution of 2-chloro-N-(pyridin-4-yl)acetamide (3.75 g, 22.0 mmol) in acetonitrile (20 mL) was added dropwise over 30 min. The reaction mixture was subsequently stirred at the same temperature for 6 h. After completion of the reaction, the volatile solvents were removed under reduced pressure, and the resulting crude solid was collected by filtration. The solid was washed with acetone (3 × 25 mL) and dried under reduced pressure at 50 °C to afford TETBA-PA as an off-white solid (98% yield). The melting point was determined to be 198–200 °C. FT-IR (KBr, cm^{-1}) showed the following characteristics: 3280 (νN–H), 1675 (νC=O, amide), 1590 (νC=N, pyridine), and 780 (νC–Cl). 1H NMR (500 MHz, DMSO-d6, ppm) provided the following chemical shifts: δ 10.45 (s, 2H, –CONHPy), 8.42 (d, J = 6.2 Hz, 4H, Py-H2,6), 8.28 (t, J = 5.5 Hz, 2H, –CONH–), 7.56 (d, J = 6.2 Hz, 4H, Py-H3,5), 4.10 (s, 4H, $–CH_2Cl$), 3.65 (d, J = 5.5 Hz, 4H, $–COCH_2NH–$), 3.32 (s, 4H, $–NCH_2CO–$), 3.12 (q, J = 6.0 Hz, 4H, $–CH_2NH–$), and 2.65–2.52 (m, 8H, central $–CH_2CH_2–$). (^{13}C NMR) (100 MHz, DMSO-d6, ppm) exhibited the following chemical shifts: δ 170.2, 168.5, 166.4, 150.3, 145.2, 113.4, 58.2, 53.4, 52.1, 42.5, and 37.8. ESI-MS m/z 683.26 [M + H]+.

3.5.4. Synthesis of DO3A-functionalized (4-pyridinyl) acetamido) appended triethylene tetramide (TETA(DO3A)$_2$-PA): A stirred solution of 1,4,7,10-tetraazacyclododecane-1,4,7-triacetic acid (DO3A; 6.93 g, 20.0 mmol, 2.0 equiv.) was prepared in deionized water (60 mL), and aqueous sodium carbonate. Subsequently, a solution of the core bis-chloroacetamide derivative TETBA-PA (6.83 g, 10.0 mmol, 1.0 equiv.) in deionized water (20 mL) was added dropwise to the stirred reaction mixture. The reaction was maintained at 60 °C for 4 h. Upon completion of the reaction, the mixture was concentrated under reduced pressure, and the resulting crude product was purified by recrystallization from water to afford TETA(DO3A)$_2$-PA as a white solid (10.42 g, 94% yield). The melting point was determined to be 210–213 °C (decomposition). 1H NMR (500 MHz): - 8.24 (d, 4H, Py-) - 7.62 (d, 4H, Py-) -3.82–3.40 (m, 20H, DO3A and other) - 3.25–2.70 (m, 44H, macrocyclic protons). 13C NMR (100 MHz): 176.2, 172.5, 170.8, 168.1, 149.2, 146.1, 114.8, 56.4, 54.8, 52.3, 51.1, 49.8, 41.6, 38.2; FT-IR-(KBr): 3420 (str)

- 1665 (carboxylate/amide I) - 1595 (pyridyl) - 1400 (str): ESI-TOF): 1187

3.5.5. Synthesis of Ruthenium (II) polypyridine moiety appended DO3A decorated (4-pyridinyl-acetamido)triethylene tetramide [TETA(DO3A)$_2$-PA((Ru(tpy-phen)$_2$)](PF$_6$)$_4$: The ligand was completely dissolved in ultrapure Milli-Q water in a round-bottom flask under continuous magnetic stirring. Subsequently, an acetonitrile solution of [Ru(II)(tpy-phen)Cl].xH_2O, was added dropwise to the reaction mixture over a period of 30 min. The reaction mixture was heated at 40 °C and continuously stirred for 12 h, followed by the addition of potassium hexafluoride salt to facilitate the formation of the stable compound. Upon completion of the reaction, the mixture was allowed to cool to room temperature. The resulting solution was purified to obtain the precursor complex [TETA(DO3A)$_2$-PA((Ru(tpy-phen)$_2$)] as a reddish-orange solid in 95% yield. FT-IR (KBr, cm-1): 3385 (br, O--H/N--H stretch), 2924 (C--H stretch), 1625 (s, C=O amide/carboxylate stretch, red-shifted), 1442 (C=C aromatic), 1085 (C--N stretch), 612 (Gd--O stretch). Elemental Analysis: Calculated for $C_{136}H_{166}Gd_2N_{34}O_{20}Ru_2$: C, 50.11; H, 5.13; N, 14.61. Found: C, 49.88; H, 5.20; N, 14.49. ESI-MS (m/z): $C_{113}H_{144}F_{24}N_{26}O_{16}P_4Ru_2]^{4+}$ [M]$^+$: 2904

3.5.6. Synthesis of [Gd(III)TETA(Gd(III)(DO3A))$_2$-PA((Ru(tpy-phen)$_2$).5H_2O](PF$_6$)$_4$: The [TETA(DO3A)$_2$-PA((Ru(tpy-phen)$_2$)](PF$_6$)$_4$ precursor metal complex was completely dissolved in ultrapure Milli-Q water in a round-bottom flask under continuous magnetic stirring. Subsequently, a 3 :1 molar ratio of an aqueous solution of gadolinium(III) chloride hexahydrate ($GdCl_3 \cdot 6H_2O$), prepared using Milli-Q water, was added dropwise to the ligand solution over a period of 30 min. The reaction mixture was heated at 40 ºC and continuously stirred for 24 h to facilitate complex formation. Throughout the reaction, the pH was monitored periodically and maintained within the range of 6.5–7.0 by the careful addition of a suitable buffering solution to neutralize the protons released during metal coordination. Upon completion of the reaction, the mixture was allowed to cool to room temperature. The resulting solution was purified to obtain the final hetero-penta-metallic complex [Gd(III)TETA(Gd(III)(DO3A))$_2$-PA((Ru(tpy-phen)$_2$).5H_2O](PF$_6$)$_4$ as a dark red-orange, hygroscopic solid in 98% yield. FT-IR (KBr, cm-1): 3385 (br, O--H/N--H stretch), 2924 (C--H stretch), 1625 (s, C=O amide/carboxylate stretch, red-shifted), 1442 (C=C aromatic), 1085 (C--N stretch), 612 (Gd--O stretch). Elemental Analysis: Calculated for $C_{136}H_{166}Gd_2N_{34}O_{20}Ru_2$: C, 50.11; H, 5.13; N, 14.61. Found: C, 49.88; H, 5.20; N, 14.49. MALDI-TOF Mass (m/z): Calculated for $C_{113}H_{148}F_{24}N_{26}O_{21}P_4Gd_3Ru_2]$ [M]$^+$: 3462.

4. Results And Discussion.

The session deals with the characterization of the precursor ligand and the target hetero pentametalic complex through various analytical spectroscopic studies.

4.1. ^{1}H NMR Spectroscopy of TETA(DO3A)$_2$-PA ligand: The most downfield singlet observed at δ 11.1 ppm is assigned to the amide proton (–NH–), which is deshielded by the adjacent carbonyl group and intermolecular hydrogen bonding. In the aromatic region (δ 7.7–7.9 ppm), two distinct doublets, each integrating for two protons, exhibit an AA′BB′ spin pattern characteristic of a para-disubstituted benzene ring (Fig.2). The downfield doublet at δ 7.9 ppm is attributed to the aromatic protons ortho to the electron-withdrawing carboxylic acid group (–COOH), whereas the doublet at δ 7.7 ppm corresponds to the protons ortho to the acetamido substituent. In the aliphatic region, a sharp singlet at δ 4.3 ppm, integrating for two protons, is assigned to the methylene group (–CH_2Cl), which is deshielded by the electronegative chlorine atom and the adjacent carbonyl group.

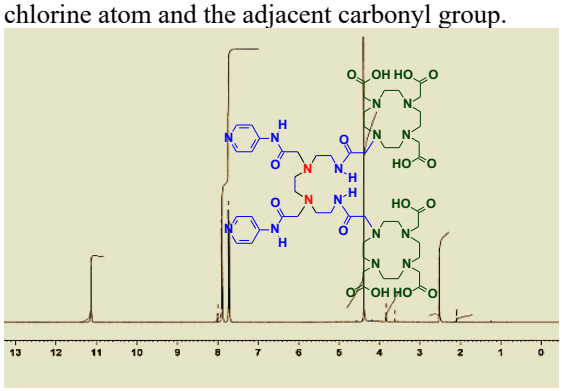

Figure-2. 500 MHz ^{1}H NMR spectrum of TETA(DO3A)$_2$-PA ligand

The residual proton signals at approximately δ 2.5 ppm and δ 3.3–3.5 ppm are attributed to DMSO-d_6 and trace water, respectively. The carboxylic acid proton (–COOH) generally appears as a broad signal at approximately δ 12–13 ppm; however, its position and visibility may vary depending on solvent, concentration, and proton exchange. The observed chemical shifts, integration values, and coupling patterns are consistent with the proposed structure of the synthesized compound.

4.2. ^{13}C NMR Spectroscopy of TETA(DO3A)$_2$-PA ligand: The ^{13}C NMR spectrum recorded at 125 MHz provides strong evidence for the proposed structure of 4-(2-chloroacetamido)benzoic acid, displaying seven distinct carbon resonances corresponding to the expected carbon environments. In the downfield region, two characteristic carbonyl signals are observed at δ 167 and 165 ppm. The resonance at δ 167 ppm is assigned to the carboxylic acid carbonyl carbon (–COOH), while the signal at δ 165 ppm corresponds to the amide carbonyl carbon (–CONH–). The aromatic region exhibits four distinct signals characteristic of the para-disubstituted benzene ring. The quaternary aromatic

carbon attached to the acetamido nitrogen (C–N) appears at δ 142 ppm, whereas the quaternary carbon bonded to the carboxylic acid substituent is observed at δ 126 ppm.

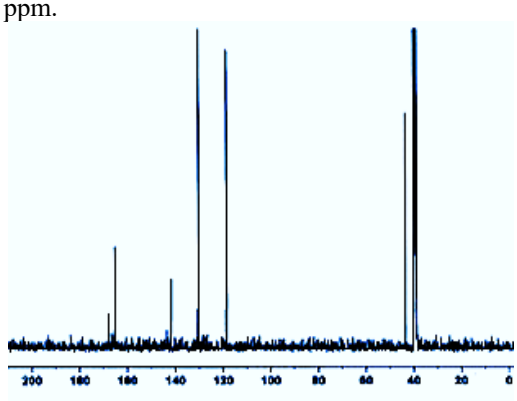

Figure-3. 125 MHz ^{13}C NMR spectrum of TETA(DO3A)$_2$-PA ligand

The two pairs of chemically equivalent aromatic CH carbons resonate at δ 131 and 119 ppm, corresponding to the protons ortho to the carboxylic acid and acetamido substituents, respectively. In the aliphatic region, the chloromethyl carbon (–CH_2Cl) exhibits a resonance at δ 43.8 ppm, consistent with the deshielding effect of the electronegative chlorine atom and the adjacent carbonyl group. Additionally, the characteristic solvent signal of DMSO-d_6 appears as a septet centred at approximately δ 39.5 ppm due to carbon–deuterium coupling. Overall, the observed chemical shifts and signal pattern are consistent with the proposed molecular structure of the TETA(DO3A)$_2$-PA ligand.

4.3. ESI Mass Spectral study of [TETA(DO3A)$_2$-PA((Ru(tpy-phen)$_2$)](PF$_6$)$_4$: The ESI-MS spectrum of the synthesized dinuclear complex exhibits a characteristic molecular ion peak at m/z 2939 (Fig.4), assigned to the species $[M+K]^+$. An additional signal at m/z 2429 is attributed to a possible adduct formation. Several intermediate fragment ions are observed at m/z 2716, 2625, 2590, and 2265, indicating partial fragmentation of the dinuclear molecular framework. Prominent fragment peaks at m/z 1801 and 1769 are attributed to the loss of macrocyclic and polypyridyl ligand components, suggesting cleavage of the coordinated molecular architecture. Another characteristic fragment at m/z 1680 is attributed to successive bond cleavage within the central polyamine–amide backbone. The base peak observed at m/z 1441 represents a particularly stable fragment generated through the breakdown of the dinuclear structure, potentially retaining one ruthenium–polypyridyl unit attached to a macrocyclic/amide fragment. Further fragmentation produces a significant signal at m/z 1327, while additional peaks at m/z 1254, 1188 and 1068 arise from lower-molecular-weight fragment ions or multiply charged species. The charge states of these ions should be established from their isotopic distributions and accurate mass measurements.

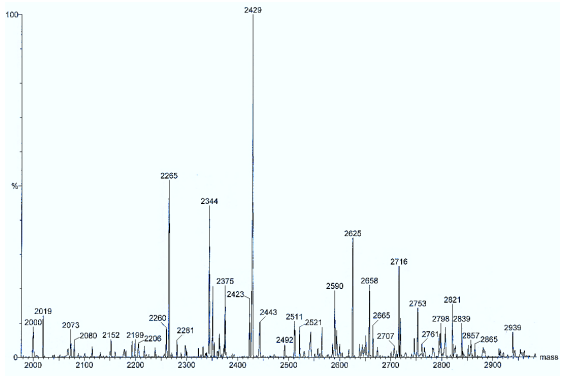

Figure-4. ESI MS spectrum of [TETA(DO3A)$_2$-PA((Ru(tpy-phen)$_2$)](PF$_6$)$_4$

4.4. MALDI-TOF Mass Spectral study of [Gd(III)TETA(Gd(III)(DO3A))$_2$-PA((Ru(tpy-phen)$_2$).5H$_2$O](PF$_6$)$_4$: The MALDI-TOF spectrum provides supporting evidence for the formation of the hetero-pentanuclear Ru(II)–Gd(III) conjugate, $[Ru_2Gd_3L]$, through the appearance of characteristic molecular ion and fragmentation signals. A prominent peak at m/z 3467 is assigned to the protonated molecular ion $[M+5H]^+$, corresponding to the intact heterometallic complex. Additional high-mass signals at m/z 2905, 2583, and 2284 are attributed to adduct formation and partial fragmentation of the parent molecular framework. The intermediate ion at m/z 2262 potentially arises from cleavage of the central amide backbone and dissociation of macrocyclic or auxiliary polypyridyl ligand components. Further fragmentation generates a heterobimetallic Ru–Gd-containing species at m/z 1940, together with lower-mass fragments at m/z 1618 and 1640, which correspond to partially dissociated metal–ligand assemblies. Additional signal at m/z 883 is attributed to lower-molecular-weight fragment ions or potentially multiply charged species. The charge states and structural assignments of these ions require confirmation through accurate-mass measurements and isotopic distribution analysis.

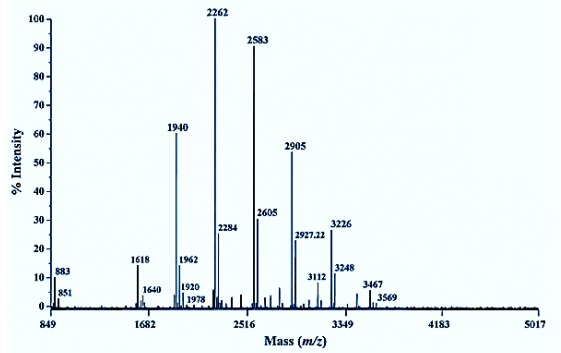

Figure-5. MALDI-TOF Mass spectrum of the target hetero-pentanuclear complex [Gd(III)TETA(Gd(III)(DO3A))$_2$-PA((Ru(tpy-phen)$_2$).5H$_2$O](PF$_6$)$_4$

4.5. Photophysical Properties of [TETA(DO3A)$_2$-PA((Ru(tpy-phen)$_2$)](PF$_6$)$_4$ Complex:

The photophysical properties of the $[TETA(DO3A)_2\text{-}PA((Ru(tpy\text{-}phen)_2)](PF_6)_4$ precursor complex were investigated by UV–Visible absorption spectroscopy in aqueous solution at 298 K (Fig.6). The absorption spectrum exhibited two bands in the wavelength range of 250–550 nm, corresponding predominantly to ligand-centred (LC) and metal-to-ligand charge-transfer (MLCT) transitions associated with the ruthenium(II) polypyridyl units. Two prominent absorption bands were observed at 295 nm, which are attributed to spin-allowed π–π* transitions involving the aromatic bipyridine, phenanthroline and pyridyl-containing ligand systems. The corresponding molar extinction coefficient is $4.25 \times 10^4\ M^{-1}\ cm^{-1}$. A broad absorption band centred at approximately 465 nm, with a molar extinction coefficient of $2.8 \times 10^4\ M^{-1}\ cm^{-1}$, was assigned to MLCT transitions involving electron transfer from the Ru(II) dπ orbitals to the π* orbitals of the coordinated ligands. The absorption tail extending towards 550 nm indicates appreciable visible-light absorption by the ruthenium-based chromophoric units. Tauc plot extrapolation yielded an apparent optical transition energy of approximately 2.42 eV, suggesting the potential of the complex for visible-light-induced photochemical applications.

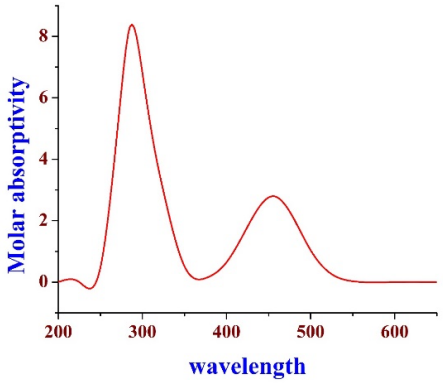

Figure-6. Absorption Spectrum of $[TETA(DO3A)_2\text{-}PA((Ru(tpy\text{-}phen)_2)](PF_6)_4$

4.6. Electronic absorption spectrum of $[Gd(III)TETA(Gd(III)(DO3A))_2\text{-}PA((Ru(tpy\text{-}phen)_2).5H_2O](PF_6)_4$ Hetero-penta-nuclear complex: The UV–Vis absorption spectrum of the complex reflects the electronic transitions associated primarily with its ruthenium–polypyridyl chromophore units (Fig.7). In the high-energy region, an intense absorption band centered at approximately 285 nm, together with a shoulder near 240 nm, is attributed mainly to intra-ligand (π→π*) transitions involving the aromatic terpyridine and 1,10-phenanthroline ligands coordinated to the Ru(II) centers. Contributions from ligand-centered transitions associated with the carboxylate and amide functionalities are also present. In the lower-energy region, a broad absorption band extending from approximately 400 to 500 nm, with a maximum near 450 nm, is characteristic of metal-to-ligand charge-transfer (MLCT) transitions, involving electron transfer from the Ru(II)-centered d orbitals to the π* antibonding orbitals of the coordinated polypyridyl ligands. The shoulder observed near 352 nm may arise from overlapping ligand-centered and charge-transfer transitions.

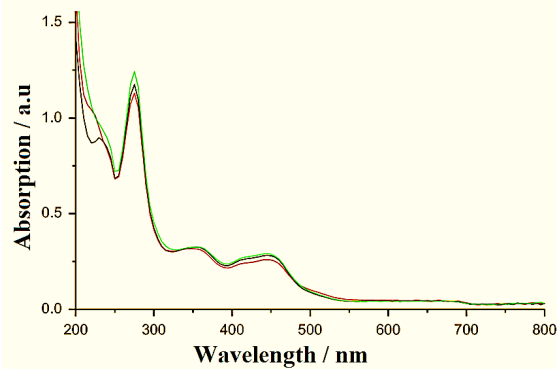

Figure-7. Absorption Spectrum of $[Gd(III)TETA(Gd(III)(DO3A))_2\text{-}PA((Ru(tpy\text{-}phen)_2).5H_2O](PF_6)_4$

Although Gd(III), with its $4f^7$ electronic configuration, exhibits weak and relatively narrow f–f transitions, its contribution to the broad absorption profile is expected to be minor compared with that of the Ru(II) chromophores. Thus, the visible-light absorption of the complex is predominantly associated with the ruthenium–polypyridyl units. The absorption band centered around 450 nm indicates the potential of the complex to utilize visible-light irradiation in photocatalytic studies. The Gd(III) centres, possessing a $4f^7$ electronic configuration, contribute predominantly to the paramagnetic properties of the complex, while their weak 4f–4f transitions have a negligible contribution to the broad visible absorption profile. Thus, the incorporation of Gd(III) through the DO3A coordination framework provides MRI-related functionality while retaining the characteristic optical absorption of the Ru(II) chromophore. These photophysical characteristics provide a basis for further investigation of the complex in optical imaging and photocatalytic applications.

4.7. Longitudinal and Transverse Relaxivity Study: The longitudinal relaxation times for the $[Gd(III)TETA(Gd(III)(DO3A))_2\text{-}PA((Ru(tpy\text{-}phen)_2).5H_2O](PF_6)_4$ at six different concentrations of the complex are presented in Table 1, Fig.8, while the graph illustrates the relationship between the concentration of the complex and 1/T1. The hetero-penta-nuclear complex shows a relaxivity of 26.43 $mM^{-1}\ s^{-1}$, which equates to 8.81 "per Gd." The "per Gd" r1p value is 2.09, 1.83, and 2.31 units greater than that of FDA-approved mononuclear Gd(III) complexes such as $[Gd(DOTA)(H_2O)]^-$ (r_{1p} = 4.2 $mM^{-1}\ s^{-1}$, 20 MHz), $[Gd(DO3A)(H_2O)_2]$ (r_{1p} = 4.8 $mM^{-1}\ s^{-1}$, 20 MHz, q =2), and $[Gd(DTPA)(H_2O)]^{2-}$ (r_{1p} = 3.8 $mM^{-1}\ s^{-1}$, 20 MHz, 25 °C), respectively.

The newly synthesized complex demonstrates higher relaxivity compared to other Gd(III) complexes such as, $[\{Gd(DO3A)\}_2L_6(H_2O)_4]$ (L6 = 2,11-dihydroxy-4,9-dioxa-1,12-dodecane) (r_{1p} = 5.1 mM^{-1} s^{-1}, 20 MHz, 40 °C), $[\{Gd(DO3A)\}_2$-L7$(H_2O)_4]$ (L7 = 1,5,6,- 10-tetrahydroxy-3,8- dioxa-dodecane) (r_{1p} = 6.4 mM^{-1} s^{-1}, 20 MHz, 40 °C), $\{Gd(DO3A)\}^{2-}$ L8$(H_2O)_4]$ (L8 = 1,2,4,5-tetrol) (r_{1p} = 6.6 mM^{-1} s^{-1}. These Gd-Ru complexes demonstrate relaxivity values that are 1.73, 1.37, and 1.33 units higher than $[Ru(phen)_2\{Gd(DOTA$-AMpy$)(H_2O)\}_2]Cl_2$ and $[Ru(ttpy)\{Gd(DOTA$-AMpy$)(H_2O)\}_3]Cl_2$. Furthermore, our Gd-Ru complexes also surpass the relaxivity of $[Ru(bpy)_2\{Gd(DOTA$-AMpy$)(H_2O)\}_2]Cl_2$, which has a reported relaxivity value of 5.80 [2,8,9,23]. This indicates a substantial improvement in its ability to enhance the MRI signal. The increased r_{1p} value is a result of five inner-sphere water molecules coordinating with the three Gd(III) ions. due to the larger molecular weight, the presence of both hydrophilic and lipophilic groups at the edges, and the high degree of rigidity in internal flexibility.

Table-1. Longitudinal Relaxivity times of the complex

Concentration (mM)	T_1 x 10^{-3} s	$1/T_1$ x 10^3 s^{-1}
0.0	3415.14	0.29
0.2	173.61	5.76
0.5	75.93	13.17
1.0	37.91	26.38
1.5	25.23	39.64
2.0	18.86	53.02
2.5	15.16	65.96

Table-2. Transverse relaxation times of the complex

Concentration (mM)	T_2 x 10^{-3} s	$1/T_2$ x 10^3 s^{-1}
0.2	0.13309	7.514
0.5	0.05323	18.785
1.0	0.02662	37.570
1.5	0.01774	56.355
2.0	0.01331	75.140
2.5	0.01065	93.925

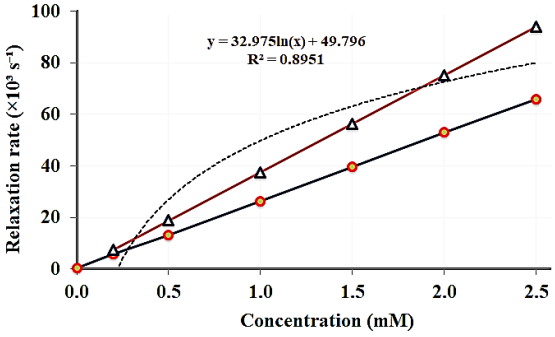

Figure-8. Concentration-Dependent Longitudinal (T_1) and Transverse (T_2) Relaxation Rates of the Heterometallic Ru(II)–Gd(III) Complex

The transverse relaxation times for six concentrations of the complex are given in Table 2, and the plot of six different concentrations of the complex from 0.2 to 2.5 Mol/L versus 1/T2 is shown in the graph. The transverse relaxivity value for the complex is found to be 37.61 mM^{-1} s^{-1}, which corresponds to 12.53 "per Gd". The higher transverse relaxivity is due to the presence of poly-pyridine groups on the periphery of the complex. The ratio r_{2p}/r_{1P} is 1.42, which shows that the complex is a T1-weighted contrast agent.

4.8. Longitudinal Relaxivity of the complex in PBS and HSA. The "per Gd" longitudinal proton relaxivity of the complex in PBS containing 4.5% HSA is 54.61 mM^{-1} s^{-1}, which is about 2.06 times higher than its relaxivity in the absence of HSA.

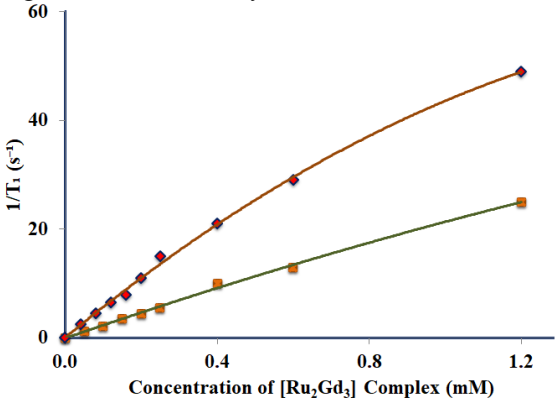

Figure-9. Concentration-Dependent Longitudinal (T_1) Relaxation Rates of the Heterometallic Ru(II)–Gd(III) Complex in PBS (Green line) and HSA (Orange line)

The increase in the longitudinal relaxivity of the complexes in the presence of HSA confirms their binding to the protein. The interaction between the complexes and HSA is confirmed by the ultrafiltration method, and the estimated association constant is *K*a = 6917 ± 658 M^{-1}, obtained by fitting the data. The number of equivalent and independent sites is set to be 1. A decrease in the mobility of the adduct formed by the complexes with HSA leads to an increase in their proton relaxation rates. The plot of the concentration of the complex versus 1/*T*1 in PBS and in the presence of HSA is depicted in the figure. 9.

4.9. Photocatalytic Degradation of Rhodamine B Dye: The heterometallic Ru(II)–Gd(III) complex is reported as a potential visible-light-active photocatalyst for the degradation of Rhodamine B (RhB) dye (Fig.10). Upon visible-light irradiation, the $[Ru(tpy)(phen)]^{2+}$ units undergo metal-to-ligand charge-transfer (MLCT) excitation, generating a long-lived triplet excited state. The excited-state electrons can participate in electron-transfer reactions with dissolved molecular oxygen, leading to the formation of reactive oxygen species (ROS), particularly superoxide radicals ($\bullet O_2^-$) and, through

subsequent reaction pathways, hydroxyl radicals (•OH). These reactive species promote the oxidative degradation of RhB molecules.

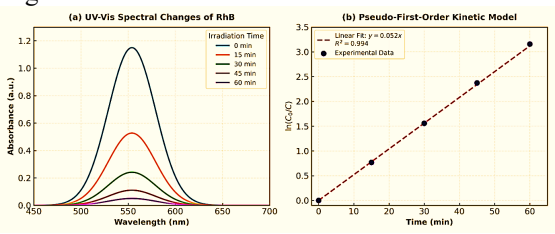

Figure-10. Photocatalytic activity of the complex against the Rhodamine B Dye

The Gd(III)–DO3A coordination units may additionally facilitate interactions with dye molecules through electrostatic and other non-covalent interactions, potentially influencing their proximity to the photosensitizing ruthenium centres. Upon irradiation for 60 min, the characteristic absorption band of RhB at approximately 554 nm exhibited a progressive decrease in intensity. The absence of a significant hypsochromic shift suggests that the degradation process may involve chromophore destruction rather than extensive stepwise N-de-ethylation. The apparent dye-binding constant of 3.45 × 10^4 M^{-1} and pseudo-first-order degradation rate constant of 0.052 min^{-1} further indicate favourable dye–catalyst interactions and efficient degradation kinetics. These observations suggest that the combination of photoactive Ru(II) centres and Gd(III)-containing coordination units may contribute to the photocatalytic performance of the heterometallic complex.

4.10. Photocatalytic Degradation of Rhodamine B, Methylene Blue, Acid Yellow Dyes: The heterometallic Ru(II)–Gd(III) supramolecular complex was investigated for its photocatalytic activity against cationic dyes, namely Rhodamine B (RhB) and Methylene Blue (MB), and the anionic dye Acid Yellow 15 (AY15) under natural sunlight irradiation (Fig.11). The photocatalytic performance was evaluated by recording time-dependent UV–Visible absorption spectra and monitoring the decrease in the characteristic absorption bands of the respective dyes. The progressive reduction in absorbance indicates the destruction of their chromophoric structures during photocatalytic treatment. The degradation efficiency was comparatively assessed to establish the influence of dye structure and charge on photocatalytic activity.

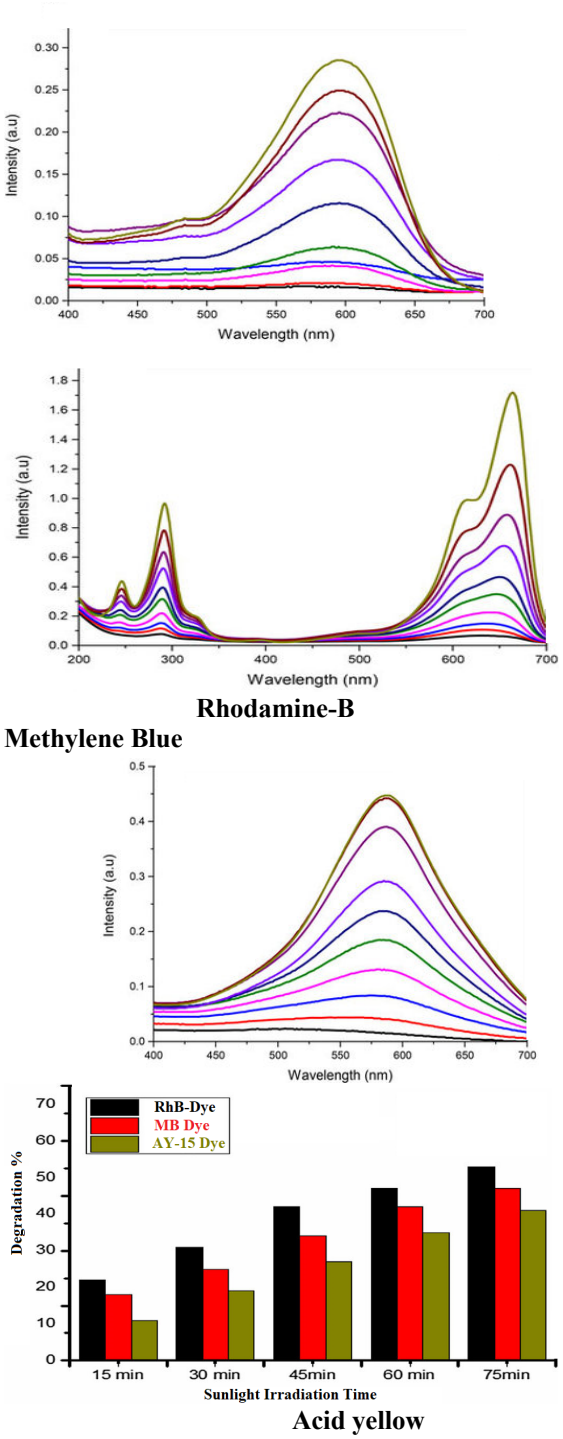

Figure-11. Photodegradation of Different Dyes by the complex under Sunlight

The differences in degradation behaviour may be associated with electrostatic interactions, aromatic stacking and the accessibility of dye molecules to the catalytic sites. Rhodamine B may interact with the aromatic polypyridyl ligands through π–π interactions, while additional non-covalent interactions may facilitate its association with the complex. Methylene Blue exhibits a different adsorption behaviour because of its cationic character and molecular structure, whereas the sulfonate groups of anionic Acid Yellow 15 may

influence its interaction with the metal-containing coordination framework. These substrate-dependent interactions can affect the adsorption equilibrium and interfacial electron-transfer processes, thereby influencing the overall degradation efficiency.

Under natural sunlight irradiation, the complex absorbs visible light and undergoes metal-to-ligand charge-transfer (MLCT) excitation, producing an excited triplet state. The excited electrons participate in electron-transfer reactions with dissolved oxygen, potentially generating reactive oxygen species (ROS), including superoxide radicals ($\bullet O_2^-$) and hydroxyl radicals ($\bullet OH$). These reactive species facilitate the oxidative degradation of adsorbed dye molecules into smaller intermediate products. The combined photophysical properties of the Ru(II) polypyridine moiety and the coordination characteristics of the Gd(III)–DO3A units contribute to the observed photocatalytic behaviour of the heterometallic complex.

5. Discussion and Future Scope

The present research and development work focuses on the design and synthesis of a novel Ru(II)–Gd(III) hetero-pentanuclear polypyridyl complex with dual-functional properties for MRI-related applications and photocatalytic wastewater treatment. The integration of ruthenium-based photosensitizing units and gadolinium-containing coordination centres offers an interesting molecular approach to combining visible-light responsiveness with magnetic relaxation properties. The promising longitudinal and transverse relaxivity values of 26.43 and 37.61 $mM^{-1}\ s^{-1}$, respectively, demonstrate its potential for further investigation as an MRI contrast-agent candidate. Additionally, its photocatalytic performance, achieving 96.8% Rhodamine B degradation under visible-light irradiation and 83% under natural sunlight, highlights its potential for organic pollutant removal.

Future research should focus on improving the photochemical stability, catalytic recyclability, and long-term aqueous stability of the complex. Detailed investigations involving reactive oxygen species identification, degradation-product analysis, toxicity assessment, and real industrial wastewater samples are essential to establish its practical applicability. Further relaxivity studies under different pH conditions, in the presence of biological macromolecules and in dye-containing solutions, would help evaluate its MRI-related performance. Ultimately, optimization, scale-up, and comprehensive biological and environmental safety assessments may facilitate the development of this multifunctional molecular system for advanced imaging and sustainable environmental remediation.

6. Conclusion

The synthesized heterometallic Ru(II)–Gd(III) complex exhibits promising magnetic relaxation and photocatalytic properties, highlighting its potential as a multifunctional molecular platform. Its longitudinal relaxivity (r_1p) of 26.43 $mM^{-1}\ s^{-1}$, equivalent to 8.81 $mM^{-1}\ s^{-1}$ per Gd(III) centre, is higher on a per-gadolinium basis than the cited mononuclear Gd(III) agents. The transverse relaxivity (r_2p) is reported as 37.61 $mM^{-1}\ s^{-1}$, giving an r_2p/r_1p ratio of 1.42; together, these values suggest suitability for further evaluation as a T_1-weighted MRI contrast candidate. In 4.5% HSA, the reported longitudinal relaxivity increases to 54.61 $mM^{-1}\ s^{-1}$, approximately 2.06-fold above the value without HSA. The association constant (K_a = 6917 ± 658 M^{-1}) supports interaction with albumin, which may slow molecular tumbling and enhance relaxation. In addition, the Ru(II) polypyridyl units promote visible-light-driven Rhodamine B degradation, with a reported apparent binding constant of $3.45 \times 10^4\ M^{-1}$ and a pseudo-first-order rate constant of 0.052 min^{-1}. These findings indicate possible applications in MRI research, image-guided studies, and photocatalytic treatment of dye-containing wastewater. Further work on relaxivity under clinically relevant field strengths, aqueous stability, toxicity, biodistribution, and validation of photocatalytic performance using real wastewater is under study.

7. Reference

1. Caravan, P., Ellison, J. J., McMurry, T. J., & Lauffer, R. B. (1999). Gadolinium(III) chelates as MRI contrast agents: Structure, dynamics, and applications. Chemical Reviews, 99(9), 2293–2352. https://doi.org/10.1021/cr980440x
2. Pushparaj, T. L., & Alexander, V. (2017). Trinuclear Gd (III) metal complex with amide core display remarkable enhancement in relaxivity. Applied Magnetic Resonance, 48, 813-825.
3. Pushparaj, L. T., & Alexander, V. (2016). Development of novel dinuclear [Gd (III) DO3VA] complexes decorated with isovaleric acid as MRI contrast agents for tumor diagnosis. International Journal of Applied Biomedical Engineering, 10, 11-17.
4. Shi, W., Song, B., Tan, M., Ye, Z., & Yuan, J. (2015). A novel heterobimetallic Ru(II)–Gd(III) complex-based magnetoluminescent agent for MR and luminescence imaging. RSC Advances, 5, 96525–96531. https://doi.org/10.1039/C5RA18544K
5. Pushparaj, L. T., & Alexander, V. (2014). Synthesis and relaxivity measurements of novel Gd (III) complex of DOTVA as MRA contrast agents. International Journal of Applied Biomedical Engineering, 8, 1-8.
6. Xiao, Y. D., Paudel, R., Liu, J., Ma, C., Zhang, Z. S., & Zhou, S. K. (2016). MRI contrast agents: Classification and application. International Journal of

Molecular Medicine, 38(5), 1319–1326. https://doi.org/10.3892/ijmm.2016.2744

7. Wahsner, J., Gale, E. M., Rodríguez-Rodríguez, A., & Caravan, P. (2019). Chemistry of MRI contrast agents: Current challenges and new frontiers. Chemical Reviews, 119(2), 957–1057. https://doi.org/10.1021/acs.chemrev.8b00363
8. Pushparaj, L. T., & Alexander, V. (2016). Synthesis, pH and HSA binding study of novel dinuclear [Gd (III) DO3VA] complex as magnetic resonance imaging contrast agent. International Journal of Scientific Engineering and Research, 7, 1600-1605.
9. Pushparaj, T. L., & Alexander, V. (2022). High rigid Gd (DO3VA) shows remarkable relaxivity: A novel class of MMI agent engineered for MR analysis. Applied Chemical Engineering, 5(1), 51-58.
10. Bafana, A., Devi, S. S., & Chakrabarti, T. (2011). Azo dyes: Past, present and the future. Environmental Reviews, 19, 350–371. https://doi.org/10.1139/a11-018
11. Hoffmann, M. R., Martin, S. T., Choi, W., & Bahnemann, D. W. (1995). Environmental applications of semiconductor photocatalysis. Chemical Reviews, 95(1), 69–96. https://doi.org/10.1021/cr00033a004
12. Saeed, M., Muneer, M., Ul Haq, A., & Akram, N. (2022). Photocatalysis: An effective tool for photodegradation of dyes—A review. Environmental Science and Pollution Research, 29, 293–311. https://doi.org/10.1007/s11356-021-16389-7
13. Pushparaj, L. T., Francy, I. R. E., & Uma, D. M. (2021). „HSA and CA-125 Binding Study of [Pr-(DO3-Ch-Ph-Am-Gd (III)) 2Pt (IV)] Complex as M-MRI Contrast Agent for Ovarian Cancer Treatment". Journal for Innovative Development in Pharmaceutical and Technical Science, 4, 1-8.
14. Khan, S., Noor, T., Iqbal, N., & Yaqoob, L. (2024). Photocatalytic dye degradation from textile wastewater: A review. ACS Omega, 9(20), 21751–21767. https://doi.org/10.1021/acsomega.4c00887
15. Pushparaj, L. P., & Sathya, S. (2021). Novel Designing of Ir (III)(Tris-Coumarin) Cored Gd (III) Complex as Targeted MRI CAs for Ovarian Cancer Treatment. Irish Interdisciplinary Journal of Science & Research (IIJSR), 5(1), 07-17.
16. Balzani, V., & Juris, A. (2001). Photochemistry and photophysics of Ru(II)–polypyridine complexes in the Bologna group: From early studies to recent developments. Coordination Chemistry Reviews, 211(1), 97–115. https://doi.org/10.1016/S0010-8545(00)00274-5
17. Pushparaj, L. P., & Rani, E. (2021). Therapeutic Properties of Gd (III)-Ir (III) Complex for Non-invasive Detection of Ovarian Cancer through M-MR Imaging. Irish Interdisciplinary Journal of Science & Research (IIJSR), 5(1), 23-33.
18. Francy Irudaya Rani, E., Lurthu Pushparaj, T., Fantin Irudaya Raj, E., & Appadurai, M. (2025). A novel boosted ada-boost classifier for MRI-based brain tumour detection. Multimedia Tools and Applications, 84(26), 30929-30950.
19. Pignatello, J. J., Oliveros, E., & MacKay, A. (2006). Advanced oxidation processes for organic contaminant destruction based on the Fenton reaction and related chemistry. Critical Reviews in Environmental Science and Technology, 36(1), 1–84. https://doi.org/10.1080/10643380500326564
20. Caravan, P., Cloutier, N. J., Greenfield, M. T., McDermid, S. A., Dunham, S. U., Bulte, J. W. M., Amedio, J. C., Jr., Looby, R. J., Supkowski, R. M., Horrocks, W. D., Jr., McMurry, T. J., & Lauffer, R. B. (2002). The interaction of MS-325 with human serum albumin and its effect on proton relaxation rates. Journal of the American Chemical Society, 124(12), 3152–3162. https://doi.org/10.1021/ja017168k
21. Juris, A., Balzani, V., Barigelletti, F., Campagna, S., Belser, P., & von Zelewsky, A. (1988). Ru(II) polypyridine complexes: Photophysics, photochemistry, electrochemistry, and chemiluminescence. Coordination Chemistry Reviews, 84, 85–277. https://doi.org/10.1016/0010-8545(88)80032-8
22. Nithyakumar, A., & Alexander, V. (2015). Synthesis, relaxivity, and in vitro fluorescence imaging studies of a novel d–f heterometallic trinuclear complex as a potential bimodal imaging probe for MRI and optical imaging. Dalton Transactions, 44(40), 17800–17809. https://doi.org/10.1039/C5DT02123E
23. Nithyakumar, A., & Alexander, V. (2016). A tri- ($Ru(II)–Gd(III)_2$) and tetranuclear ($Ru(II)–Gd(III)_3$) d–f heterometallic complexes as potential bimodal imaging probes for MRI and optical imaging. New Journal of Chemistry, 40, 4606–4616. https://doi.org/10.1039/C5NJ03393D